Thin Solid Films 763 (2022) 139601

Contents lists available at ScienceDirect

Thin Solid Films

journal homepage: www.elsevier.com/locate/tsf

Optimization of reactive ion beam sputtered Ta_2O_5 for III–V compounds

Jarno Reuna *, Marianna Vuorinen, Riku Isoaho, Arto Aho, Severi Mäkelä, Arttu Hietalahti, Elina Anttola, Antti Tukiainen, Mircea Guina

Optoelectronics Research Centre, Physics Unit, Faculty of Engineering and Natural Sciences, Tampere University, P.O. Box 692, Tampere FIN-33014, Finland

ARTICLE INFO

Keywords:
Ion beam sputtering
Tantalum pentoxide
Optimization
III–V semiconductors
Solar cells

ABSTRACT

We report the optimization of the process parameters used in ion beam sputtering of dielectric Ta_2O_5 thin films on III–V semiconductor surfaces, with an aim of minimizing the deterioration of semiconductor surfaces and their opto-electric performance. We demonstrate that linear tuning of the three main sputtering parameters, namely, the primary source radiofrequency power, the ion beam current, and the ion beam voltage, allows optimizing the deposition conditions of Ta_2O_5 minimizing the damage to the III–V surfaces. The effect of parametrization is evaluated by deposition of a Ta_2O_5 antireflection coating on GaAs-based multijunction solar cells employing AlGaAs and AlInP window layers. Numerical study reveals that the main source of damage is the scattered primary ions, in this case argon ions, that have not contributed to the sputtering process of the Ta_2O_5 at the target. Moreover, it is likely that the reactive oxygen atmosphere oxidizes the semiconductor surfaces in the initial phase of the deposition process. A similar optimization procedure should be employed for any other thin film directly deposited by reactive ion beam sputtering on III–V surfaces and optoelectronics devices to avoid deposition induced damage.

1. Introduction

Ion beam sputtering (IBS) is a coating method for producing high quality optical thin films with high laser damage threshold and environmentally stable optical constants [1,2]. Widely used IBS materials include oxides (SiO_2, TiO_2, Al_2O_3, Ta_2O_5) [3–6] and nitrides (SiN_x, TiN_x, AlN) [7–10]. The oxides and nitrides can be produced with reactive ion beam sputtering utilizing a reactive gas atmosphere, optionally backed with additional oxygen or nitrogen radicals for ensuring stoichiometric growth of films [4,6,11,12]. The energetic sputtering process enables production of high quality films in near room temperature [6,9,10], which is a distinct advantage of IBS when compared to other physical vapor deposition methods of dielectrics, usually requiring sample heating or additional kinetic energy provided by an ion source beaming directly on the substrates by ion assisted deposition [13,14].

IBS processes are well established for coating optical filters on top of glass substrates [15] and the process control parameters are typically matched for high uniformity, high growth rate, and high film quality, namely smooth surface topography, stable optical constants, and good adhesion. When IBS is used for thin film deposition on optoelectronic devices, the coated surface differs from glass, creating a need for re-optimization of the process parameters to avoid process related damages of the semiconductor surface. In addition to adhesion and optical properties of the coating, the effects of deposition on the material properties of the semiconductor devices should be considered.

In this study we focus on optimizing the IBS processes involved in deposition of antireflection coatings (ARC) on III–V multijunction solar cells (MJSC). Such MJSCs exhibit high conversion efficiencies providing that sunlight is transmitted into the cell without reflection losses over a broadband spectrum, which may extend from UV to beyond 1.5 μm [16]. A relatively high refractive index of ~2 and low absorption at wavelengths above ~300 nm [12] makes tantalum pentoxide (Ta_2O_5) a promising dielectric material for this purpose. However, utilizing IBS grown Ta_2O_5 as the starting layer of the ARC is not a viable option without re-optimization of the deposition process to ensure that the semiconductor surface is not critically damaged by the deposition process. Besides reporting on the parametrization of Ta_2O_5 thin films to be used for ARC on III–V MJSCs, we employ a numerical analysis to evaluate the cause of IBS induced deterioration of the semiconductor surface.

2. Methods

The Ta_2O_5 films were deposited using a Navigator 700 (Cutting Edge

* Corresponding author.
E-mail address: jarno.reuna@tuni.fi (J. Reuna).

https://doi.org/10.1016/j.tsf.2022.139601
Received 20 May 2022; Received in revised form 4 October 2022; Accepted 17 November 2022
Available online 19 November 2022

Coatings GmbH) reactive ion beam sputtering system. Sputtering was performed using Ar:O_2 mixture with flow rates of 8 sccm to 5 sccm, respectively. A 200 mm × 200 mm tantalum (Ta) plate with a purity of 99.95% was used as a sputtering target. The deposition took place in a reactive O_2 atmosphere with a pressure of 4.5 × 10^{-2} Pa. The distance from target to substrate was 0.4 m and the substrates were mounted on a planar substrate holder. The main sputtering parameters, namely primary source radiofrequency (RF) power, the ion beam current (I_{beam}) and the ion beam voltage (U_{beam}), were varied to optimize the film growth. The sputtering parameters used for the parametrization series are presented in Table 1. During the deposition, the sample holder was rotated at 60 rpm to guarantee uniform film deposition.

A test series of Ta_2O_5/SiO_2 ARCs using the parametrized Ta_2O_5 were deposited on top of two different lattice-matched GaAs-based triple-junction solar cell structures: GaInP/GaAs/GaInNAsSb with AlInP window layer and AlGaAs/GaAs/GaInNAsSb with AlGaAs window layer. The solar cells were grown by molecular beam epitaxy on p-GaAs substrates using a Veeco GEN20 MBE system. The wafers were diced into 6 mm × 6 mm solar cells with an active area of 0.25 cm^2. The diced wafer pieces served as photoluminescence samples and the actual solar cell devices were further processed by depositing Ni/Au (10/100 nm) front contact grid on the n-side and Ti/Au (50/100 nm) planar back contact on the p-side by an electron beam evaporator. Different window materials used for the structures enable comparison between oxidized and non-oxidized sample surfaces, as AlGaAs is prone to form a native oxide under O_2 atmosphere, whereas the oxidation of AlInP is a slower process [17]. Prior to deposition, the n-type contact GaAs layers were removed by wet etching with NH_3:H_2O_2:H_2O solution to expose the window layers. Beside the solar cell samples, the parametrized Ta_2O_5 layers were also deposited on rectangular 8 mm × 8 mm silicon (Si) and n-GaAs (100) substrates for ellipsometric and atomic force microscope characterizations. These samples were diced from 2″ wafers with nominal thicknesses of 325 μm and 625 μm for Si and GaAs, respectively. In order to verify the possible surface topography changes in the semiconductor material resulting from the coating process, the Ta_2O_5 layers on the n-GaAs test samples were wet etched with 50% hydrofluoric acid (HF) for 30 s, rinsed with de-ionized water and dried with nitrogen blow. A Dimension™ 3100 Atomic force microscope (AFM) from Veeco Ltd was used to obtain topographical information and surface roughness of the Ta_2O_5 layers and the post-deposition HF etched GaAs surfaces. The AFM image data was constructed with WSxM 5.0 Develop 9.4 software [18].

Film thickness and refractive index of the Ta_2O_5 films were determined with a Rudolph AutoEL III Null ellipsometer utilizing a He/Ne laser at $\lambda = 632.8$ nm. The parameters for ellipsometric calculations were the refractive index of Si-substrate $n_S = 3.863$, substrate extinction coefficient $k_S = 0.162$ and 70° angle of incidence.

For assessing the effects of the deposition parameters of Ta_2O_5 on the III–V materials, an Accent RPM2000 photoluminescence (PL) mapper was used to measure the PL from the top and middle junctions of the MJSC structures. The GaInP and AlGaAs top junctions were probed with 532 nm laser both in continuous wave (CW) and Q-switched modes using a 300 g/mm grating, a 570 nm high-pass filter, and a CCD detector. The effects on the GaAs junction were evaluated by measuring the PL with CW 785 nm excitation using a 300 g/mm grating, an 850 nm high-pass filter, and an InGaAs detector.

Table 1
Sputtering parameters for the Ta_2O_5 test series. Parameter f denotes the linear scaling coefficient for the three ion source parameters.

f	Primary Source RF Power [W]	Beam Current [mA]	Beam Voltage [V]
1	145	225	2000
0.9	131	203	1800
0.8	116	180	1600
0.7	102	158	1400
0.6	87	135	1200
0.5	73	113	1000

Light-biased current-voltage (LIV) characteristics of the solar cells were measured using a 7 kW OAI TriSol solar simulator calibrated for AM1.5D (1000 W/m^2) illumination. Open-circuit voltage (V_{OC}) and short-circuit current density (J_{SC}) obtained from the LIV measurements were used to compare the device performance. A PerkinElmer Lambda 1050 UV/VIS/NIR spectrophotometer equipped with a Universal Reflectance Accessory (URA) module was used for the reflectance measurements. The URA measures the specular reflectance at 8° angle of incidence.

Sputtering has a well-established theoretical background for which Sigmund linear cascade collision model [19] provides a basis on which many others have built their improved models [20–22]. Applying these is often done using numerical Monte Carlo simulations run by programs such as SDTrimSP [23], TRIDYN [24] and SRIM [25]. In this work, we used the semi-empirical sputtering equations reported by Seah et al. [21] (Eq. (B.4)–(B.11) and (B.16)–(B.19)) and recommended values used by Matsunami et al. [26] (Eq. (B.12)–(B.15)). These provide a simplistic, yet proven and efficient model for sputtering compounds [27]. For oblique incident angle calculations, we used the approach reported by Yamamura et al. [28] (Eq. (B.20)–(B.26)). The main calculational result describing a sputtering event is the sputtering yield Y, which refers to the ratio of the number of the sputtered particles per a projectile ion. Calculating the sputtering yield of a specific compound requires considering the surface binding energy of the compound, the collision cross-sections and energy transfers of all the included particles, the sputtering threshold of the projectile-target pair, and the initial energy of the sputtering projectiles. The theory and the equations are presented as supplementary material in Appendix B.

Although the initial Ta target is metallic, based on previous studies we can assume that the surface of the target is oxidized [12,29] and that the molecular species being sputtered is Ta_2O_5. Demiryont et al. [12] showed that after the oxygen fraction of the ion beam exceeds 37.5% the sputtered Ta_2O_5 film is stoichiometric, and in their experiments they did not use additional background oxygen. The oxygen fraction for the ion beam used in this work is 38.5% and there is a constant 80 sccm O_2 flow directed to the target plate, which according to Ohno et al. [29] already induces several nanometers thick oxide layer on the target. Fig. 1 presents simplified schematics of the main sputtering process under evaluation. We have chosen to examine the sputtering of TaO subparticles instead of Ta_2O_5, as it simplifies the calculations and includes the effects for having both oxygen and tantalum atoms in the sputtered species. A further analysis of the specific distribution of the possible particles present in the sputtered yield (Ta, TaO_2, TaO_3, Ta_2O_5) is not considered here.

In this simplified scheme, the following effects are neglected:

(I) sputtering by the oxygen ions present at the ion beam,
(II) possible preferential sputtering of oxygen or tantalum at the target surface, and
(III) the presence of sputtered species other than TaO molecules,

The assumptions are made to simplify the calculations. The simplifications are justified by the assumption that (I) the oxygen in the ion beam mainly contributes via oxidizing reactions with tantalum or as O_2^+ ions, which has a mass similar to Ar^+ ion (36 u versus 40 u, respectively), (II) the empirical comparison by Seah [27] shows that the preferential effects can be neglected in the used model, and (III) the TaO should represent an average example of the possible species fit to describe the phenomenon on a very general level.

In addition to the sputtering at the target surface, we also numerically examine the possible secondary sputtering effects of the semiconductor samples by the scattered Ar^+ ions and the TaO primary particles prior to the formation of the initial Ta_2O_5 layers. The secondary TaO particle energies are calculated assuming elastic two particle collisions, as has been done by Bundesmann [30], Feder [31], and Lautenschläger [32] [Eq. (B.28) and (B.29)]. The semiconductor

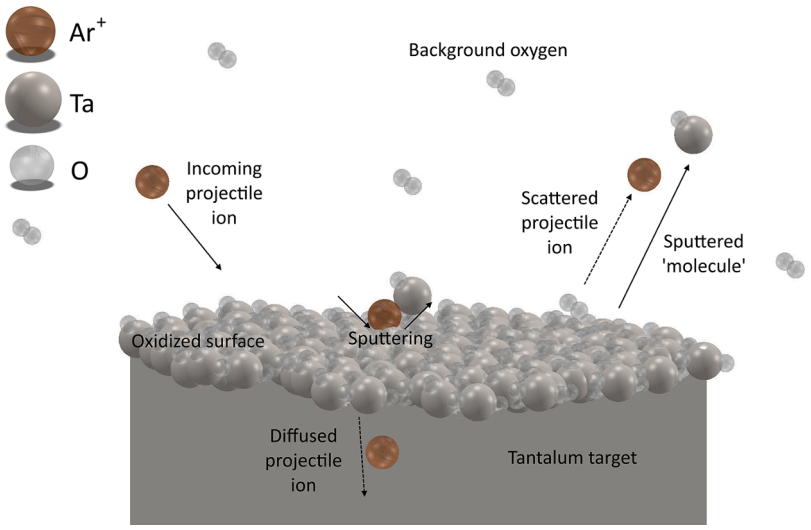

Fig. 1. A simplified illustration of the reactive sputtering process at the Ta target surface.

sputtering calculations rely equally on Seah's compound equations [27] and Malherbe's review on sputtering semiconductors [22]. The energy distribution of sputtered TaO particles is calculated with the flux equations introduced by Thompson [33] [Eq. (B.30)–(B.39)]. The sputtering yields are calculated for GaAs, $Al_{0.53}In_{0.47}P$ and $Al_{0.4}Ga_{0.6}As$ compositions and their properties are assumed to be linearly constructed by the properties of their binary compounds. Such simplification omits any element preferential effects and might not represent the actual sputtering process of these compounds, as is emphasized also by both Seah [27] and Malherbe [22]. The models used, however, have been experimentally verified for GaAs and Ta_2O_5 and they do reveal the overall trend of the processes they describe. Regarding ternary compounds there is very little sputtering data available for experimental verification of the model, so the numerical estimations should be taken as a rough approximation. The compositions for AlInP and AlGaAs calculations are selected to match the window materials used, i.e. $Al_{0.53}In_{0.47}P$ and $Al_{0.8}Ga_{0.2}As$.

3. Results and discussion

The calculated growth rates and measured refractive indices at 632.8 nm obtained from the ellipsometry measurements of the parametrized Ta_2O_5 films are shown in Fig. 2a). The linear tuning of the ion source parameters results in almost linear scaling for the growth rate. Only the standard parameters ($f = 1$) result in slightly larger growth rate than expected by the linear fit. As we are restricted by the system parameters, higher than $f = 1$ parametrizations are not possible. Therefore, there remains a question if the trend of growth rate would stop being linear with higher U_{beam}. The refractive index of the films varies significantly (~0.05) between the different parametrizations but does not clearly follow any trend. It is still inconclusive that how some of the excluded variables in the test series (e.g. system condition prior deposition and short-term coating history) affect in the results. Nevertheless, it can be said that when changing Ta_2O_5 parametrization, care must be taken to verify the corresponding refractive index of the material as it cannot be linearly scaled or presumed to be constant in respect to the scaling factor.

Fig. 2b) shows the calculated sputtering yields for Ta_2O_5 as a function of the kinetic energy of the argon projectiles ($E_{proj} \approx U_{beam}$) at the normal incidence and at the sputtering angle of 55° used in this work. The vertical lines indicate the parametrization values and are marked for $f = 1$, 0.7, 0.6, 0.5 that are further examined with the MJSC ARCs. The sputtering yield increases along with the sputtering angle and the projectile energy. Within the energy range of the parametrization ($E_{proj} =$ 1000–2000 V), the sputtering yield can be approximated to be linear, which is analogous with the growth rates shown in Fig. 2a). The reduction in yield with the investigated parametrized values compared to the standard deposition is more than 1 atom/ion, which can be considered as a notable difference.

PL is a non-invasive characterization method, which allows versatile evaluation of MJSC devices by using variable excitation depths [34,35]. PL intensity generally indicates the quality of surfaces, bulk and interfaces [36,37] and when the reflectance changes are considered and the signal normalized according to the pre-deposition signal, the intensities should be ≥ 1 for non-damaged samples. A comparison of the effects of the parametrization on PL is shown in Fig. 3. Excitation with 532 nm probes the topmost junction, either GaInP or AlGaAs, and CW mode mainly generates signal from the very topmost part of the junction, whereas Q-switched enables signal contribution from deeper in the junction. The 785 nm excited signal comes from the middle GaAs junction.

The results in Fig. 3 show that the standard sputtering parameters for Ta_2O_5 degrade the material quality of both MJSC structures independent of the window layer material. It seems that the top junction takes most of the damage with the standard parameters ($f = 1$) as the GaAs signal remains above 1, while the PL of the top junctions drops significantly. For $f = 0.7$ the AlInP window MJSC has already significantly improved surface PL when compared to the standard parametrization, but for AlGaAs the PL is just slightly better. At $f = 0.6$ all the signals are above 1 indicating unharmful deposition of Ta_2O_5 in respect of the MJSCs. For $f = 0.5$, however, the signal from AlGaAs top junction is reduced for CW excitation. All the other signals are slightly better or the same than with the parametrization $f = 0.6$. The overall trend seems to be that the PL intensities improve as the sputtering parameters are reduced. Only contradiction to this is the drop of the AlGaAs PL intensity from $f = 0.6$ to $f = 0.5$. As the Q-switched signal is still relatively high (~1.4), the signal drop of AlGaAs could be related to oxidation of the AlGaAs window layer of the top junction. This could also explain why the signal for AlInP window structure is further improved, as AlInP does not oxidate similarly than AlGaAs.

As the Ta_2O_5 films are expected to be amorphous [5], it is unlikely to have drastic topographical differences in the parametrized series. Nevertheless, to rule out the possible effect of structural differences of Ta_2O_5 layers, the parametrized films were investigated with AFM. The surface topography maps are shown in Fig. 4.

The dielectric nature of Ta_2O_5 causes slight areal charging effect during the AFM scans and the resulting maps are not the sharpest in contrast. Despite this, the scans shown in Fig 4 represent relatively well

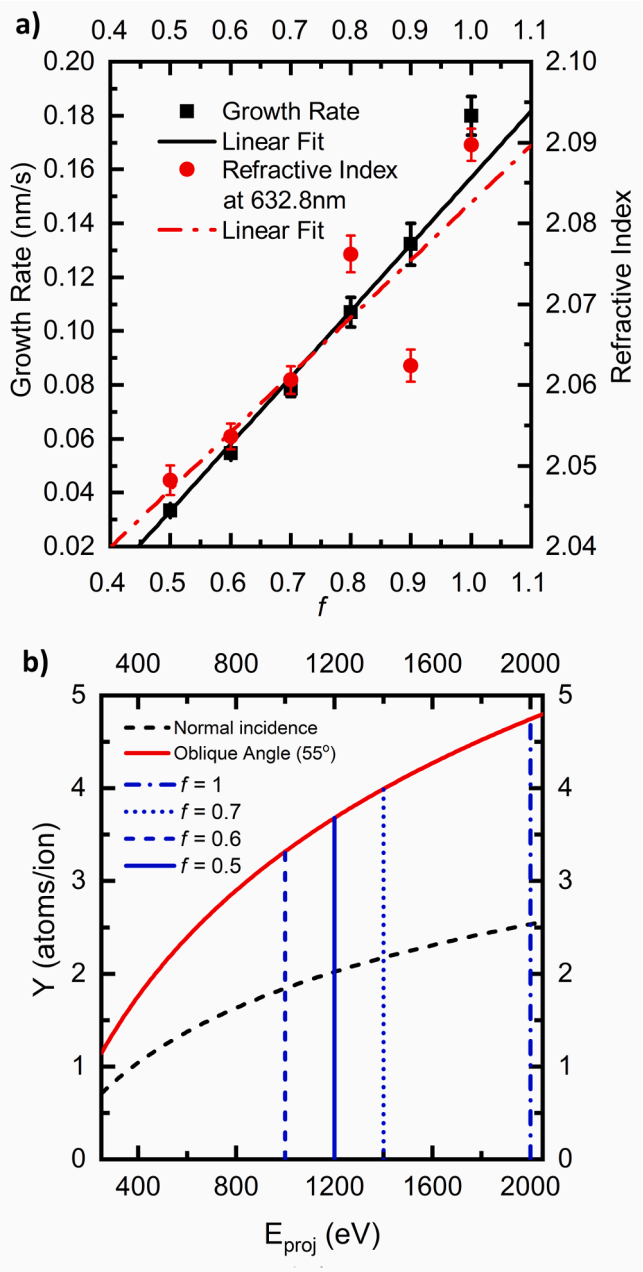

Fig. 2. a) Growth rate and refractive index as a function of the scaling factor *f*. The uncertainty bars represent 90% level of confidence. b) Numerically calculated sputtering yield (Y) of Ta_2O_5 with Ar^+ ions (E_{proj}) for normal incidence and for the incidence angle of 55° used in this work.

the overall quality of the Ta_2O_5 surfaces. Based on the topography maps, there is no significant difference in the surface quality between the parametrized films as the root-mean-square roughness R_{rms} and average roughness R_{ave} values are almost identical between the samples. The roughness values show that there is only a minor difference in the sputtered oxide film smoothness for standard parameters ($f = 1$) film compared to the parametrized films. This could be related to the roughening of the semiconductor surface in the beginning of the coating process. All the films are very smooth, both R_{rms} and R_{ave} being ~0.1 nm, and the parametrization does not significantly affect the surface quality of the films. This indicates that the differences in the PL results would come solely from the semiconductor material and not from changes in the Ta_2O_5 films. Possible damage mechanisms include unintentional sputtering of the III–V surface by the scattered primary projectiles (Ar^+) or the sputtered molecules (TaO), ion implantation of the scattered Ar^+ ions, and crystal defects induced by collision cascades.

Fig. 5a) shows the calculated (Eq. (B.28)-(B.29)) maximum kinetic energies of the sputtered TaO particles and the scattered argon ions as a function of the primary ion energy. From this it would seem equally likely for the sputtering of the semiconductor material to be caused either by the Ar^+ ions or the sputtered TaO species.

Fig. 5b) shows the calculated (Eq. (B.30)-(B.39)) fluxes of the sputtered TaO particles as a function of the particle energy, both in low energy region ($\leq$ 50 eV) and in high energy region ($\geq$ 50 eV). Majority of TaO particles has less than 50 eV kinetic energy to begin with and on their way to the substrate they lose most of their kinetic energy due to collisions with the background gas particles [38]. On average, a sputtered TaO particle collides approximately 4 times (Eq. B.30–32) with oxygen before reaching the semiconductor surface, whereas a scattered Ar^+ ion undergoes only ~2 collisions. The collisions have been calculated for oxygen atmosphere, where other gas species have not been considered. In this sense, the post-collision energies shown in Fig. 5a) and b) are the absolute upper limits for projectiles arriving at the substrates.

In addition to the projectile energetics, the surface binding energies (U_{sb}) of the sputtered material needs to be known to estimate the possible secondary sputtering at the semiconductor surface. Although U_{sb} has a strong effect on the sputtering yields, the used values are usually just approximations like the heat of sublimation or the heat of atomization of the material under investigation. In this work the values have directly been taken from Seah [27] and Malherbe [22]. With the U_{sb} values and the information of the projectiles, the sputtering threshold for each target-projectile combination can be calculated. There are different ways to calculate the sputtering threshold energies and here the equations of Matsunami [26] and Yamamura [28] have been used for normal incidence and oblique angle sputtering thresholds, respectively. The sputtering thresholds are provided in Table 2. Values calculated with Bohdansky's formulation [20] have also been provided, which are commonly used as a simple approach to estimate sputtering thresholds and yields.

When comparing the values in Table 2, there are some variations depending on the method used for calculating the threshold. However, the overall magnitude for each of the target-projectile combination is of the same order, excluding the oblique angle values that should be lower due to larger fraction of particle energy deposited near surface when compared to normal incidence [30]. Projectiles with less energy than the sputtering threshold of the material do not contribute to the sputtering process. Therefore, the relevant quantity for TaO flux is the number of particles having more kinetic energy than 50 eV. Table 3 shows the integrated TaO fluxes above 50 eV and their fractions of the total TaO flux.

The integrated fluxes are large enough that they need to be taken into consideration in the yield calculations. However, the higher sputtering threshold energies indicate smaller yields compared to Ar^+. In contrast, the sputtering threshold energies with Ar^+ are about ~10 eV smaller than for TaO. The number of scattered Ar^+ ions can be significant and their high-energy counts can be ten times of the counts for high-energy sputtered species [39,40], which would favor sputtering by the Ar^+ ions compared to TaO particles. The calculated sputtering yields for Ar^+ ions are shown in Fig. 6a) and for TaO particles in Fig. 6b).

The angular sputtering yields are not well defined with the projectile energies below and near the threshold energy of the target materials [28], so the calculated yields for TaO sputtering are shown $E_{spu} \geq 50$ eV, which is well above the calculated sputtering thresholds for oblique angles in Table 2. It can be stated that the yields follow the sputtering threshold energies i.e., the lowest threshold material (GaAs) has the highest yield and so forth. Also, the yields with Ar-projectiles are nearly three times higher than the yields by TaO particles with the same parametrization. This combined with the thermalization losses that the TaO particles experience on their way from target to samples [38] makes it more likely that the damage for the semiconductors is due to the

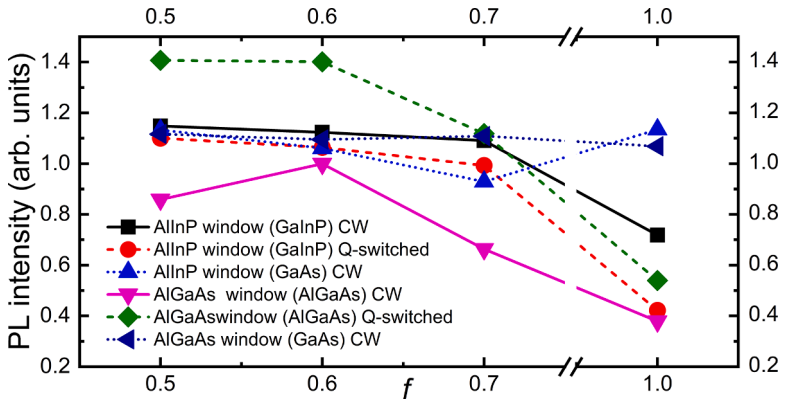

Fig. 3. Normalized reflectance-corrected PL intensities from the MJSC structures with AlGaAs or AlInP window layer coated with the parametrized Ta_2O_5 ARCs.

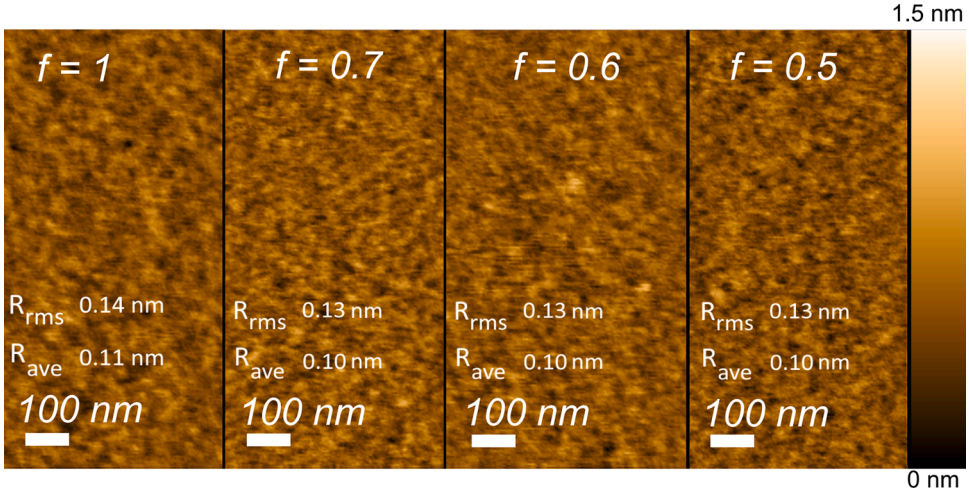

Fig. 4. Surface topography maps of the parametrized Ta_2O_5 thin films by AFM.

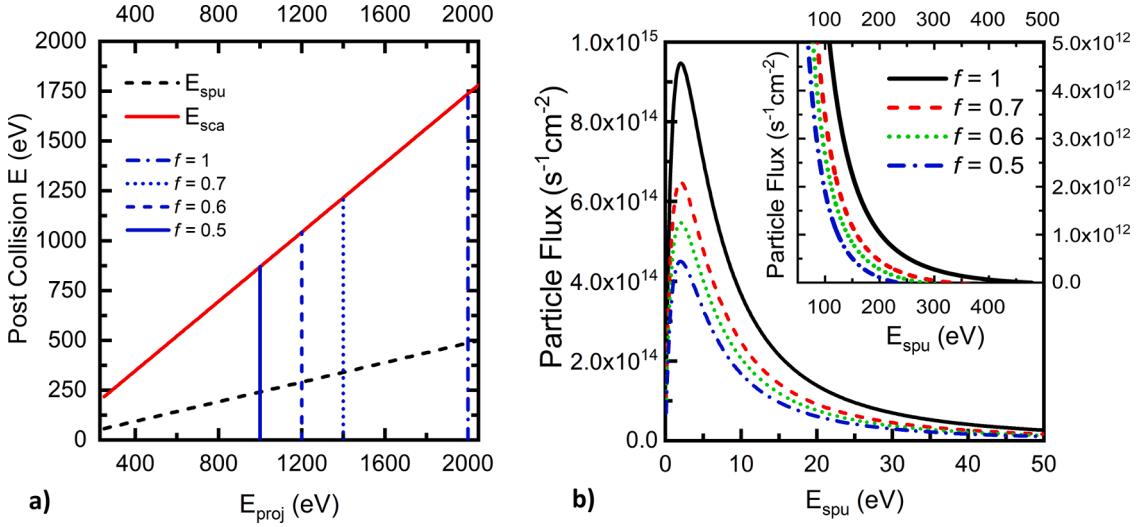

Fig. 5. a) Calculated maximum kinetic energies of the sputtered TaO particles (E_{spu}) and the scattered Ar ions (E_{sca}). b) Calculated fluxes of the sputtered TaO particles as a function of the particle energy, both in low energy region ($\leq$ 50 eV) and in high energy region ($\geq$ 50 eV).

scattered Ar^+ ions. The differences in PL results with parametrization are not directly explained by the sputtering yield as both AlInP and AlGaAs follow similar trend between $f = 1$ and $f = 0.5$, so it is likely that the surface oxidation of AlGaAs plays a major role in the discrepancies between the two window materials.

To verify the possible surface topography changes in the semiconductor material caused by the coating process, a test series of parametrized Ta_2O_5 films on n-GaAs samples were wet etched with 50%

Table 2
Calculated sputtering thresholds for Ta_2O_5, GaAs, AlGaAs and AlInP.

Sputtering Threshold [eV]							
Target material	Ta_2O_5	GaAs		AlGaAs		AlInP	
Projectile	Ar^+	Ar^+	TaO	Ar^+	TaO	Ar^+	TaO
$E_{th}^{Matsunami}$	19	14	41	16	49	23	77
$E_{th}^{Bohdansky}$	28	21	40	24	45	33	63
$E_{th}^{Yamamura}$	42	19	45	21	53	39	59
$E_{th}^{Oblique}$	14	8	19	9	22	16	24

Table 3
Integrated TaO particle fluxes of particles having over 50 eV kinetic energy and their relative amount in comparison to total TaO particle flux.

f	Integrated Flux [$s^{-1}cm^{-2}$] $E_{spu} \geq 50$ eV	Relative Amount from Total Flux
1	9.8×10^{15}	8.4%
0.7	5.5×10^{15}	7.1%
0.6	4.1×10^{15}	6.4%
0.5	2.8×10^{15}	5.4%

HF to remove the Ta_2O_5 layers. The nominal etch rate of Ta_2O_5 in 50% HF is ~230 nm/min [41], so the films with the thickness of 39 nm should have been completely dissolved with the treatment. GaAs is used in place of the MJSCs, as HF is known to etch Al-containing III–V materials rapidly [42–44], which would prevent observing any surface changes caused by the deposition on AlInP or AlGaAs surfaces. The AFM scans for the post-deposition HF-etched n-GaAs samples are shown in Fig. 7. Also, a non-etched GaAs sample was measured, but it proved to be topographically identical with the HF etched sample and thus is not shown here.

The results show that with $f = 1$, the semiconductor surface gets little rougher (0.01 nm) when compared to the just etched GaAs, which indicates only minor secondary sputtering taking place at the sample surface. Noteworthy, the difference in Ta_2O_5 layer roughness for standard parametrization compared to other parametrizations shown in Fig 4. corresponds with the increase in roughness observed with the HF etched $f = 1$ GaAs sample. For $f = 1$ there are visible islands with heights of ~3 nm and diameters ranging between 10 and 50 nm. Such islands are also visible on the just HF-etched GaAs and $f = 0.6$ sample, but their diameters are only of ~15 nm with heights of ~1 nm. In order to deduce the formation mechanism of the larger islands, their elemental composition should be analyzed. At this point, it is assumed that the reactive O_2 atmosphere produces native oxides [45,46] that have different surface binding energies from non-oxidized semiconductor material, which leads to preferential sputtering. The islands on $f = 0.5$ sample are of the same diameter (~15 nm) than on the just HF-etched and $f = 0.6$ samples, but slightly lower in height (~0.5 nm), which makes them almost indistinguishable on the scan. The parametrized films $f = 0.6$ and $f = 0.5$ seem to produce smoother surfaces than the HF-etched reference GaAs, which could be either caused by slight sputtering of any loosely bound surface atoms, or densification of the surface species. It is possible that the present oxygen species in the reactive sputtering process can affect the former by creating more volatile compounds on the semiconductor surface. In addition, the parametrization $f = 0.5$ produces even smoother surface than $f = 0.6$, which partially contradicts the PL results shown in Fig. 3, where the surface PL gets worse for the AlGaAs window structure with $f = 0.5$. As the smaller scaling parameter decreases the growth rate of Ta_2O_5 and thus increases the time the bare semiconductor surface is exposed to the reactive oxygen species, we believe that the deterioration of PL for AlGaAs surface is more due to the surface oxidation than the deposition parameters related to secondary sputtering. This notion is backed by the PL results of the other junctions being better with the $f = 0.5$ than $f = 0.6$, and the sputtering yields for AlInP and AlGaAs following similar trend between $f = 0.5$ than $f = 0.6$ for both investigated projectile species.

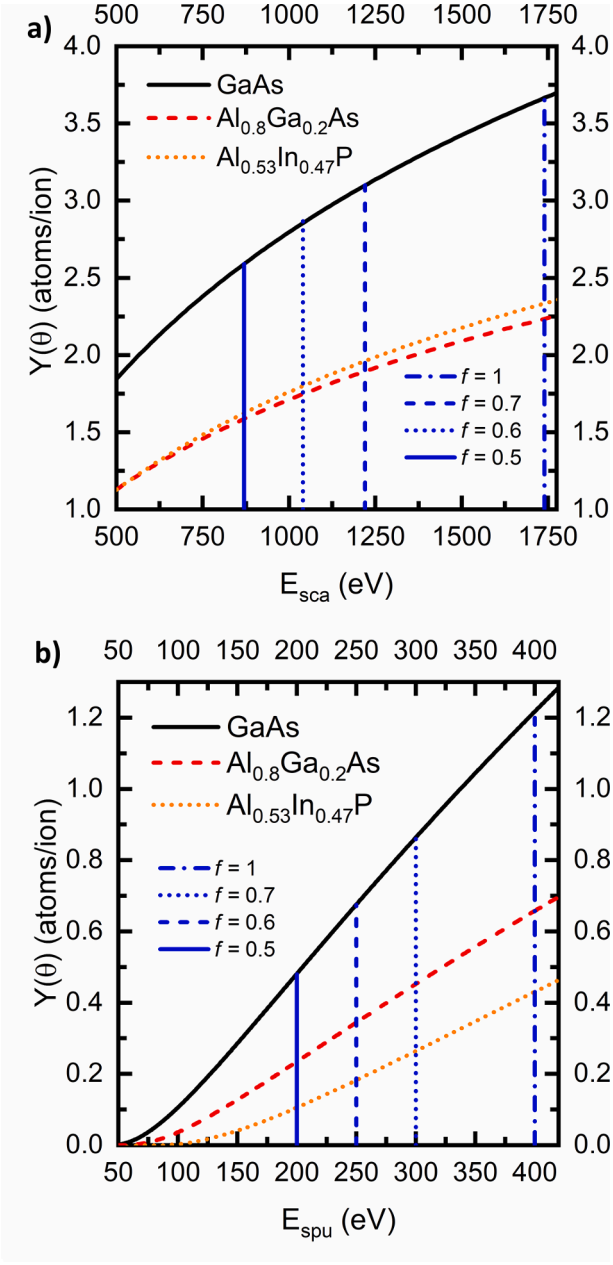

Fig. 6. a) Calculated sputtering yields for GaAs, AlGaAs and AlInP by the scattered Ar^+ ions at 50° incidence. b) Calculated sputtering yields for GaAs, AlGaAs and AlInP by the primary TaO particles at 50° incidence.

Photoluminescence and surface quality alone do not demonstrate the effects of Ta_2O_5 parametrization on a MJSC device performance. For this GaInP/GaAs/GaInNAsSb MJSCs were coated with Ta_2O_5/SiO_2 ARCs with the standard parameters ($f = 1$) and the best parametrization result by PL ($f = 0.6$). Just the starting Ta_2O_5 layers of the ARCs are parametrized. The corresponding LIV results of the MJSCs are shown in Fig. 8a).

The negative effect of standard Ta_2O_5 coating on the cell performance is drastic, as it provides worse LIV performance than the uncoated MJSC, although its average reflectance is 20 percentage points lower. This indicates deposition inherited damage to the solar cell structure that increases recombination losses. The parametrized ARC in comparison leads to a significant enhancement in the current density (~40%) and shows no clear evidence of coating process induced damage. Moreover, the open-circuit voltage does not vary between the MJSCs, being ~2.6 V for all three, which points mainly to increased recombination losses in the window layer, instead of other loss

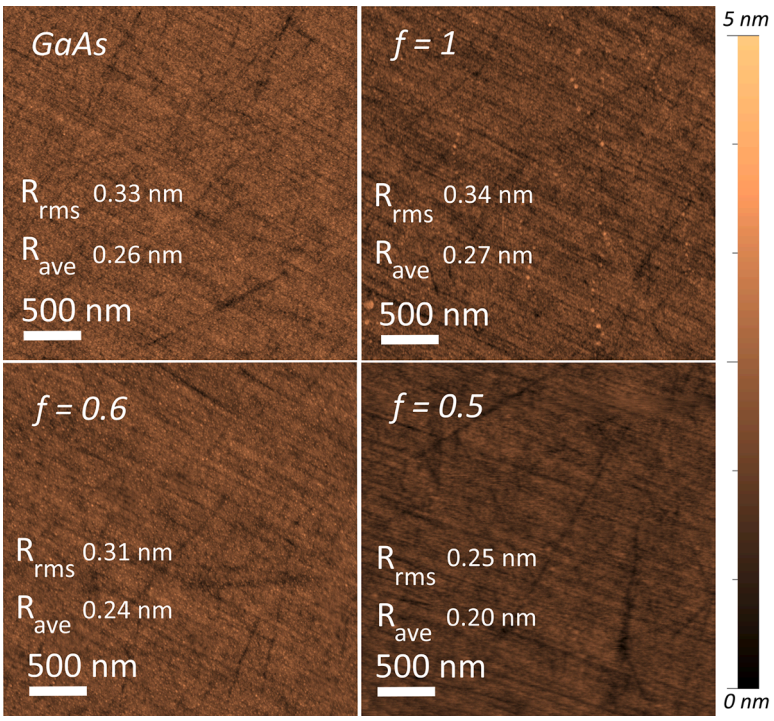

Fig. 7. AFM surface topography maps of the n-GaAs samples after post-deposition HF etching of parametrized Ta_2O_5 thin films and just HF etched GaAs as a reference.

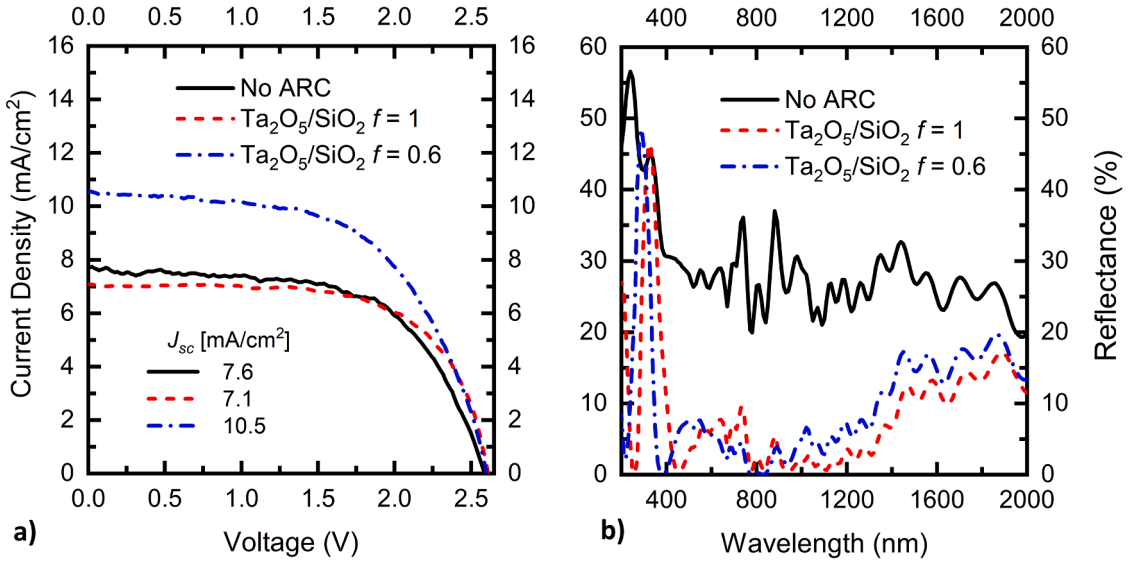

Fig. 8. a) Demonstration of the effects of parametrization of Ta_2O_5 on GaInP/GaAs/GaInNAsSb MJSC light-biased current-voltage properties with an uncoated MJSC, and with ARCs deposited using $f = 1$ and $f = 0.6$ parametrizations. The measured current densities, shown under the curves, highlight the influence of parametrization on the MJSC performance. b) Measured reflectance of GaInP/GaAs/GaInNAsSb MJSCs without an ARC and with the parametrized ARCs.

mechanisms. The reflectance in Fig. 8b) show that both ARCs provide similar improvement in reflectivity compared to the uncoated MJSC, although small differences can be seen due to nominally different refractive index of Ta_2O_5 layer and minor alteration in layer thicknesses between the coating runs. Based on the LIV results, non-optimal parametrized deposition of Ta_2O_5 is not suitable for optoelectronics, as it clearly causes functional damage to the semiconductor materials. Similarly, it is seen that optimization mitigates the deposition induced degradation.

4. Conclusions

Optimization of the process parameters use in reactive ion beam sputtering of Ta_2O_5 thin films for III–V multijunction solar cells was investigated in order to prevent deposition induced damage of the semiconductors. The parametrized Ta_2O_5 was used as a starting layer for an ARC on both GaInP/GaAs/GaInNAsSb and AlGaAs/GaAs/GaInNAsSb MJSCs with AlInP and AlGaAs window layers, respectively.

The standard deposition parameters were found to damage the MJSCs leading to reduced PL intensities and to a significant drop in the short-circuit current density, by 0.5 mA/cm^2 when compared to an

uncoated MJSC, and by 3.4 mA/cm^2 when compared to the ARC with the optimized parameters. The parametrization was done by linearly scaling the three main parameters of the ion source, namely RF power, ion beam current, and beam voltage.

Numerical investigations indicate that the root cause for the performance drop is caused by the scattered Ar^+ions that have not contributed to the target sputtering. AFM comparison revealed a slight increase in the surface roughness with the standard parameters that is due to secondary sputtering of the semiconductor surface. The scaled parameters provided smoother surfaces than the non-coated reference GaAs. It is likely that the surface oxidation plays a significant role in the observed secondary sputtering and performance changes in the MJSC. Future work needs to address the oxidation of the semiconductor surfaces and the possible preferential sputtering that was omitted here.

The linear parametrization provided a functional tool to find suitable deposition conditions of Ta_2O_5 for III–V multijunction solar cells. We see it necessary to utilize such parametrization for all IBS materials deposited on III–V semiconductors to prevent surface damage and device degradation. For further improvement we would suggest pre-deposition passivation to prevent uncontrolled oxidation of the semiconductor surface. This would remove one unknown variable (state of oxidation) from the process and would allow more specific deposition process optimization for specific coated semiconductor compound.

CRediT authorship contribution statement

Jarno Reuna: Conceptualization, Methodology, Software, Investigation, Visualization, Writing – original draft. **Marianna Vuorinen:** Conceptualization, Investigation. **Riku Isoaho:** Conceptualization, Writing – review & editing. **Arto Aho:** Conceptualization, Writing – review & editing, Supervision, Project administration. **Severi Mäkelä:** Investigation. **Arttu Hietalahti:** Investigation, Writing – review & editing. **Elina Anttola:** Investigation, Writing – review & editing. **Antti Tukiainen:** Writing – review & editing, Funding acquisition. **Mircea Guina:** Writing – review & editing, Supervision, Funding acquisition.

Declaration of Competing Interest

The authors declare that they have no known competing financial interests or personal relationships that could have appeared to influence the work reported in this paper.

Data availability

Data will be made available on request.

Supplementary materials

Supplementary material associated with this article can be found, in the online version, at doi:10.1016/j.tsf.2022.139601.

References

[1] L. Gallais, B. Mangote, M. Commandré, M. Mende, L. Jensen, H. Ehlers, M. Jupé, D. Ristau, A. Melninkaitis, V. Sirutkaitis, S. Kičas, T. Tolenis, R. Drazdys, An exhaustive study of laser damage in ion beam sputtered pure and mixture oxide thin films at 1030nm with 500 fs pulse durations, 8530 (2012) 85300K–85300K–8. 10.1117/12.977553.

[2] D. Ristau, T. Gross, Ion beam sputter coatings for laser technology, Adv. Opt. Thin Film II 5963 (2005), 596313, https://doi.org/10.1117/12.624772.

[3] J.R. Sites, P. Gilstrap, R. Rujkorakarn, Ion beam sputter deposition of optical coatings, Opt. Eng. (1983) 22, https://doi.org/10.1117/12.7973141.

[4] P. Shang, S. Xiong, L. Li, D. Tian, W. Ai, Investigation on thermal stability of Ta2O5, TiO2and Al2O3coatings for application at high temperature, Appl. Surf. Sci. 285 (2013) 713–720, https://doi.org/10.1016/j.apsusc.2013.08.115.

[5] M. Cevro, Ion-beam and dual-ion-beam sputter deposition of tantalum oxide films, Opt. Eng. 34 (1995) 596, https://doi.org/10.1117/12.188616.

[6] M. Cevro, G. Carter, Ion beam sputtering and dual ion beam sputtering of titanium oxide films, J. Phys. D Appl. Phys. 28 (1995) 1962–1976, https://doi.org/10.1088/0022-3727/28/9/026.

[7] H.-J. Erler, G. Reisse, C. Weissmantel, Nitride film deposition by reactive ion beam sputtering, Thin Solid Films 65 (1980) 233–245, https://doi.org/10.1016/0040-6090(80)90257-6.

[8] P. Martin, R. Netterfield, W. Sainty, Optical properties of TiNx produced by reactive evaporation and reactive ion-beam sputtering, Vacuum 32 (1982) 359–362, https://doi.org/10.1016/0042-207X(82)93829-5.

[9] M.F. Lambrinos, R. Valizadeh, J.S. Colligon, Effects of bombardment on optical properties during the deposition of silicon nitride by reactive ion-beam sputtering, Appl. Opt. 35 (1996) 3620, https://doi.org/10.1364/AO.35.003620.

[10] H.Y. Chen, S. Han, H.C. Shih, The characterization of aluminum nitride thin films prepared by dual ion beam sputtering, Surf. Coat. Technol. 200 (2006) 3326–3329, https://doi.org/10.1016/j.surfcoat.2005.07.046.

[11] H. Demiryont, J.R. Sites, Effects of oxygen in ion-beam sputter deposition of titanium oxides, J. Vac. Sci. Technol. A 2 (1984) 1457–1460, https://doi.org/10.1116/1.572383.

[12] H. Demiryont, J.R. Sites, K. Geib, Effects of oxygen content on the optical properties of tantalum oxide films deposited by ion-beam sputtering, Appl. Opt. 24 (1985) 490, https://doi.org/10.1364/AO.24.000490.

[13] P.J. Martin, A. Bendavid, M. Swain, R.P. Netterfield, T.J. Kinder, W.G. Sainty, D. Drage, L. Wielunski, Properties of thin films of tantalum oxide deposited by ion-assisted deposition, Thin Solid Films 239 (1994) 181–185, https://doi.org/10.1016/0040-6090(94)90848-6.

[14] J.J. McNally, K.C. Jungling, F.L. Williams, J.R. McNeil, Optical coatings deposited using ion assisted deposition, J. Vac. Sci. Technol. A 5 (1987) 2145–2149, https://doi.org/10.1116/1.574940.

[15] T.W. Jolly, R. Lalezari, Ion-beam sputter deposition techniques for the production of optical coatings of the highest quality, in: K.H. Guenther (Ed.), SPIE Thin Film Opt. Syst., 1993: p. 250. 10.1117/12.141036.

[16] D.J. Friedman, Progress and challenges for next-generation high-efficiency multijunction solar cells, Curr. Opin. Solid State Mater. Sci. 14 (2010) 131–138, https://doi.org/10.1016/j.cossms.2010.07.001.

[17] S. Van Riesen, A.W. Bett, Degradation study of III-V solar cells for concentrator applications, Prog. Photovolt. Res. Appl. 13 (2005) 369–380, https://doi.org/10.1002/pip.603.

[18] I. Horcas, R. Fernández, J.M. Gómez-Rodríguez, J. Colchero, J. Gómez-Herrero, A. M. Baro, WSXM: a software for scanning probe microscopy and a tool for nanotechnology, Rev. Sci. Instrum. 78 (2007) 1–8, https://doi.org/10.1063/1.2432410.

[19] P. Sigmund, Theory of sputtering. I. Sputtering yield of amorphous and polycrystalline targets, Phys. Rev. 184 (1969) 383–416, https://doi.org/10.1103/PhysRev.184.383.

[20] J. Bohdansky, A universal relation for the sputtering yield of monatomic solids at normal ion incidence, Nucl. Instruments Methods Phys. Res. Sect. B Beam Interact. with Mater. Atoms 2 (1984) 587–591, https://doi.org/10.1016/0168-583X(84)90271-4.

[21] M.P. Seah, C.A. Clifford, F.M. Green, I.S. Gilmore, An accurate semi-empirical equation for sputtering yields I: for argon ions, Surf. Interface Anal. 37 (2005) 444–458, https://doi.org/10.1002/sia.2032.

[22] J.B. Malherbe, Sputtering of compound semiconductor surfaces. I. Ion-solid interactions and sputtering yields, Crit. Rev. Solid State Mater. Sci. 19 (1994) 55–127, https://doi.org/10.1080/10408439408244588.

[23] W. Eckstein, R. Dohmen, A. Mutzke, R. Schneider, SDTrimSP: a Monte-Carlo code for calculating collision phenomena in randomized targets, (2007). http://hdl.handle.net/11858/00-001M-0000-0027-04E8-F.

[24] W. Möller, W. Eckstein, Tridyn—a TRIM simulation code including dynamic composition changes, Nucl. Instrum. Methods Phys. Res. Sect. B 2 (1984) 814–818, https://doi.org/10.1016/0168-583X(84)90321-5.

[25] J.F. Ziegler, M.D. Ziegler, J.P. Biersack, SRIM—the stopping and range of ions in matter (2010), Nucl. Instrum. Methods Phys. Res. Sect. B 268 (2010) 1818–1823, https://doi.org/10.1016/j.nimb.2010.02.091.

[26] N. Matsunami, Y. Yamamura, Y. Itikawa, N. Itoh, Y. Kazumata, S. Miyagawa, K. Morita, R. Shimizu, H. Tawara, Energy dependence of the ion-induced sputtering yields of monatomic solids, At. Data Nucl. Data Tables 31 (1984) 1–80, https://doi.org/10.1016/0092-640X(84)90016-0.

[27] M.P. Seah, T.S. Nunney, Sputtering yields of compounds using argon ions, J. Phys. D Appl. Phys. 43 (2010), 253001, https://doi.org/10.1088/0022-3727/43/25/253001.

[28] Y. Yamamura, Y. Itikawa, N. Itoh, Angular Dependence of Sputtering Yields of Monatomic Solids, Institute of Plasma Physics, Nagoya University, Nagoya, Japan, 1983.

[29] T. Ohno, S. Samukawa, Resistive switching in a few nanometers thick tantalum oxide film formed by a metal oxidation, Appl. Phys. Lett. 106 (2015), 173110, https://doi.org/10.1063/1.4919724.

[30] C. Bundesmann, H. Neumann, Tutorial: the systematics of ion beam sputtering for deposition of thin films with tailored properties, J. Appl. Phys. 124 (2018), 231102, https://doi.org/10.1063/1.5054046.

[31] R. Feder, F. Frost, H. Neumann, C. Bundesmann, B. Rauschenbach, Systematic investigations of low energy Ar ion beam sputtering of Si and Ag, Nucl. Instrum. Methods Phys. Res. Sect. B 317 (2013) 137–142, https://doi.org/10.1016/j.nimb.2013.01.056.

[32] T. Lautenschlager, Systematic Investigation of the Ion Beam Sputter Deposition of TiO2, University of Leipzig, 2018. Ph.D. Thesis, https://nbn-resolving.org/urn:nbn:de:bsz:15-qucosa2-321567.

[33] M.W. Thompson II, The energy spectrum of ejected atoms during the high energy sputtering of gold, Philos. Mag. 18 (1968) 377–414, https://doi.org/10.1080/14786436808227358.
[34] H. Nesswetter, P. Lugli, A.W. Bett, C.G. Zimmermann, Electroluminescence and photoluminescence characterization of multijunction solar cells, in: 2012 IEEE 38th Photovoltaic Specialists Conference (PVSC) PART 2, IEEE, 2012, pp. 1–6, https://doi.org/10.1109/PVSC-Vol2.2012.6656769.
[35] D. Lan, J.F. Geisz, M.A. Steiner, I. Garcia, D.J. Friedman, M.A. Green, Improved modeling of photoluminescent and electroluminescent coupling in multijunction solar cells, Sol. Energy Mater. Sol. Cells 143 (2015) 48–51, https://doi.org/10.1016/j.solmat.2015.06.036.
[36] F. Trespidi, A. Malchiodi, F. Farina, Note: Photoluminescence measurement system for multi-junction solar cells, Rev. Sci. Instrum. 88 (2017), 056104, https://doi.org/10.1063/1.4982586.
[37] J. García-García, J. González-Hernández, J.G. Mendoza-Alvarez, E.L. Cruz, G. Contreras-Puente, Photoluminescence characterization of the surface layer of chemically etched CdTe, J. Appl. Phys. 67 (1990) 3810–3814, https://doi.org/10.1063/1.346055.
[38] K. Meyer, I.K. Schuller, C.M. Falco, Thermalization of sputtered atoms, J. Appl. Phys. 52 (1981) 5803–5805, https://doi.org/10.1063/1.329473.
[39] R. Feder, C. Bundesmann, H. Neumann, B. Rauschenbach, Ion beam sputtering of Ag—angular and energetic distributions of sputtered and scattered particles, Nucl. Instrum. Methods Phys. Res. Sect. B 316 (2013) 198–204, https://doi.org/10.1016/j.nimb.2013.09.007.
[40] D. Kalanov, A. Anders, C. Bundesmann, Ion beam sputtering of silicon: energy distributions of sputtered and scattered ions, J. Vac. Sci. Technol. A. 37 (2019), 051507, https://doi.org/10.1116/1.5114973.
[41] C. Christensen, R. de Reus, S. Bouwstra, Tantalum oxide thin films as protective coatings for sensors, in: Technical Digest. IEEE International MEMS 99 Conference. Twelfth IEEE International Conference on Micro Electro Mechanical Systems (Cat. No.99CH36291), IEEE, 1999, pp. 267–272, https://doi.org/10.1109/MEMSYS.1999.746832.
[42] S.J. Pearton, Critical issues of III–V compound semiconductor processing, Mater. Sci. Eng. B 44 (1997) 1–7, https://doi.org/10.1016/S0921-5107(96)01744-8.
[43] G.J. Bauhuis, P. Mulder, E.J. Haverkamp, J.C.C.M. Huijben, J.J. Schermer, 26.1% thin-film GaAs solar cell using epitaxial lift-off, Sol. Energy Mater. Sol. Cells 93 (2009) 1488–1491, https://doi.org/10.1016/j.solmat.2009.03.027.
[44] C.W. Cheng, K.T. Shiu, N. Li, S.J. Han, L. Shi, D.K. Sadana, Epitaxial lift-off process for gallium arsenide substrate reuse and flexible electronics, Nat. Commun. 4 (2013) 1–7, https://doi.org/10.1038/ncomms2583.
[45] N.A. Torkhov, Formation of a native-oxide structure on the surface of n-GaAs under natural oxidation in air, Semiconductors 37 (2003) 1177–1184, https://doi.org/10.1134/1.1619513.
[46] R. Toyoshima, S. Murakami, S. Eguchi, K. Amemiya, K. Mase, H. Kondoh, Initial oxidation of GaAs(100) under near-realistic environments revealed by in situ AP-XPS, Chem. Commun. 56 (2020) 14905–14908, https://doi.org/10.1039/D0CC05279E.